DOI: 10.1007/s11099-018-0781-0 PHOTOSYNTHETICA 56 (1): 217-228, 2018

The multiplicity of roles for (bi)carbonate in photosystem II operation in the hypercarbonate-requiring cyanobacterium *Arthrospira maxima*‡

G. ANANYEV[*,**], C. GATES[*,**], and G.C. DISMUKES[*,**,+]

The Waksman Institute of Microbiology[*] and Department of Chemistry and Chemical Biology[**], Rutgers University, Piscataway, NJ 08854, USA

Abstract

Arthrospira maxima is unique among cyanobacteria, growing at alkaline pH (<11) in concentrated (bi)carbonate (1.2 M saturated) and lacking carbonic anhydrases. We investigated dissolved inorganic carbon (DIC) roles within PSII of *A. maxima* cells oximetrically and fluorometrically, monitoring the light reactions on the donor and acceptor sides of PSII. We developed new methods for removing DIC based on a (bi)carbonate chelator and magnesium for (bi)carbonate ion-pairing. We established relative affinities of three sites: the water-oxidizing complex (WOC), non-heme iron/Q_A^-, and solvent-accessible arginines throughout PSII. Full reversibility is achieved but (bi)carbonate uptake requires light. DIC depletion at the non-heme iron site and solvent-accessible arginines greatly reduces the yield of O_2 due to O_2 uptake, but accelerates the PSII–WOC cycle, specifically the S2→S3 and S3→S0 transitions. DIC removal from the WOC site abolishes water oxidation and appears to influence free energy stabilization of the WOC from a site between CP43-R357 and Ca^{2+}.

Additional key words: bicarbonate depletion; dissolved inorganic carbon; oxygen-evolving complex; redox tuning; water-oxidizing complex.

Introduction

The vast majority of oxygenic photosynthesis in the biosphere takes place under atmospheric, CO_2-limited conditions, using no more than the current 400 ppm CO_2 (Drake *et al.* 1997). Most phototrophs grow poorly or not at all in concentrated CO_2 gas, and in the case of aquatic phototrophs, concentrated dissolved inorganic carbon (DIC, often as bicarbonate). In contrast to most oxygenic phototrophs, the cyanobacterium *Arthrospira maxima* (formerly *Spirulina maxima*) is capable of sustained growth under the highest possible DIC concentrations, ranging from atmospheric conditions to 1.2 M total bicarbonate in its native alkaline lake habitats (Vonshak and Tomaselli 2000). In evolving this strong alkaline tolerance (growth at pH 11.5 can occur), *A. maxima* shed the genes for carbonic anhydrases involved in carbon-concentrating mechanisms (Hillier *et al.* 2006). It has adapted a specificity for (bi)carbonate uptake rather than carbon dioxide, utilizing bicarbonate transporters to control its distribution in cells and store energy as ion gradient. *A. maxima* is widely used for biomass production, as it grows quickly, reaching yields up to 3 g L^{-1}, can be grown on flue gas-enriched carbonate media, exhibits robust stress tolerance, and the pH of medium is toxic to many parasites and fungi (Carrieri *et al.* 2007). It is a unique prokaryotic photoautotroph for studies of the multiplicity of roles that DIC has in metabolism.

Received 23 May 2017, *accepted* 8 September 2017, *published as online-first* 15 January 2018.
+Corresponding author; e-mail: dismukes@rutgers.edu
Abbreviations: alpha – miss; beta – double hit; Chl – chlorophyll; delta – backward transition; DIC – dissolved inorganic carbon; DMBQ – 2,5-dimethyl-*p*-benzoquinone; epsilon – deactivation; F_0 – minimal fluorescence yield of the dark-adapted state; F_m – maximal fluorescence yield of the dark-adapted state; FRRF – fast repetition rate fluorometry; F_v – variable fluorescence; F_v/F_m – maximal quantum yield of PSII photochemistry; PET – photosynthetic electron transport; PQ – plastoquinone; S0–S4 – oxidation states of the WOC, "S-states"; VZAD (model) – Vinyard-Zachary-Ananyev-Dismukes model; WOC – water oxidizing complex; Yss – steady-state yield.
Acknowledgements: This work was funded by the Department of Energy, Basic Energy Sciences, Grant DE-FG02-10ER16195, and by the Stanford University Global Climate and Energy Project, activity number 96. We thank Dr. Dmitry Shevela for constructive advice and previous research, Prof. A. W. Rutherford for research which provided a foundation for our own work, and Prof. Govindjee for a long lifetime of progress on this subject and a great deal of prior advice.
‡Dedicated to Prof. Govindjee on the occasion of his 85th birthday.

Here we focused on the roles of (bi)carbonate in PSII operation of *A. maxima*.

PSII is the water oxidizing enzyme that produces O_2 as byproduct while delivering 4 H atoms to plastoquinone. It is easily photodamaged and can act as a source of reactive oxygen species formed by donor and acceptor side reactions; it is therefore highly regulated. Scheme 1 provides a map of the locations and summarizes the purported functional roles of five of the DIC-affected targets in PSIIs and during biogenesis of the $CaMn_4O_5$ core comprising the water-oxidizing complex (WOC) by the process known as photoassembly (also known as photoactivation). The functional roles of DIC within PSII have been studied since the earliest (disproven) speculated role for bicarbonate as the electron donor and source of evolved O_2 by Otto Warburg. A thorough history has been given by Shevela *et al.* (2012).

(Bi)carbonate has been consistently found coordinated to the non-heme iron atom located between the first (Q_A) and second (Q_B) plastoquinone electron carriers (Ferreira *et al.* 2004, Shen 2015). The non-heme iron ligating site of (bi)carbonate was first qualitatively identified by Govindjee and coworkers and has been extensively demonstrated and further localized by his group and others (Wydrzynski and Govindjee 1975, Vermaas and Rutherford 1984, Diner *et al.* 1991). The dissociation constant of bicarbonate from the non-heme iron site was recently established to be pH-dependent (van Rensen *et al.* 1999, Koroidov *et al.* 2014, Brinkert *et al.* 2016). The specific function it influences, transfer of electrons from Q_A^- to Q_B, was elucidated by Govindjee *et al*. (Govindjee and van Rensen 1993) and subsequently confirmed in (Snel and van Rensen 1984). This led to the hypothesis for a possible regulatory role (Govindjee and van Rensen 1993, van Rensen *et al.* 1999). A further function of bicarbonate as a "proton shuttle" for delivery to reduced Q_B *via* non-heme iron has been proposed (Govindjee and van Rensen 1993). Until recently bicarbonate was believed to be irreplaceable at this site (Roach *et al.* 2013). Recently, DIC depletion was shown to shift the electrochemical reduction potential of the Q_A/Q_A^- couple by +75 mV *in vitro* (Brinkert *et al.* 2016), though the location of the site(s) involved were not established.

The evidence for multiple DIC functions supporting donor-side reactions is extensive, although this complexity and low binding affinity has led to less clear consensus on the number and location of DIC sites of action (Shevela *et al.* 2012). Here we single out three in Scheme 1*C* and 1*D*. While (bi)carbonate has been excluded as a potential electron donor to the WOC (Clausen *et al.* 2005, Hillier *et al.* 2006), evidence consistently indicates DIC interacts with various small lumenal subunits of PSII that aid in photoprotection of the WOC (Klimov and Baranov 2001). Additionally, (bi)carbonate anions can associate specifically with positively charged arginine groups *via* combined ion-pairing and hydrogen-bonding forces. There are over one hundred arginines distributed throughout the inner and outer surfaces of PSII that are potential binding sites for carbonate. Their role in proton conduction is described below. Bicarbonate is the terminal base for neutralization of protons released during water oxidation in some strains, notably *Arthrospira maxima*, Scheme 1*C*, Eqs. 1 and 2 (Carrieri *et al.* 2007, Shevela *et al.* 2008). Evidence indicates this proton neutralization function may account for the significantly faster O_2 evolution rate (4×) at light saturation by *Arthrospira maxima vs*. conventional oxygenic phototrophs (Ananyev and Dismukes 2005, Ananyev *et al.* 2016).

CP43-arginine357 is located in the second coordination shell of the WOC and the mutant replacing positive

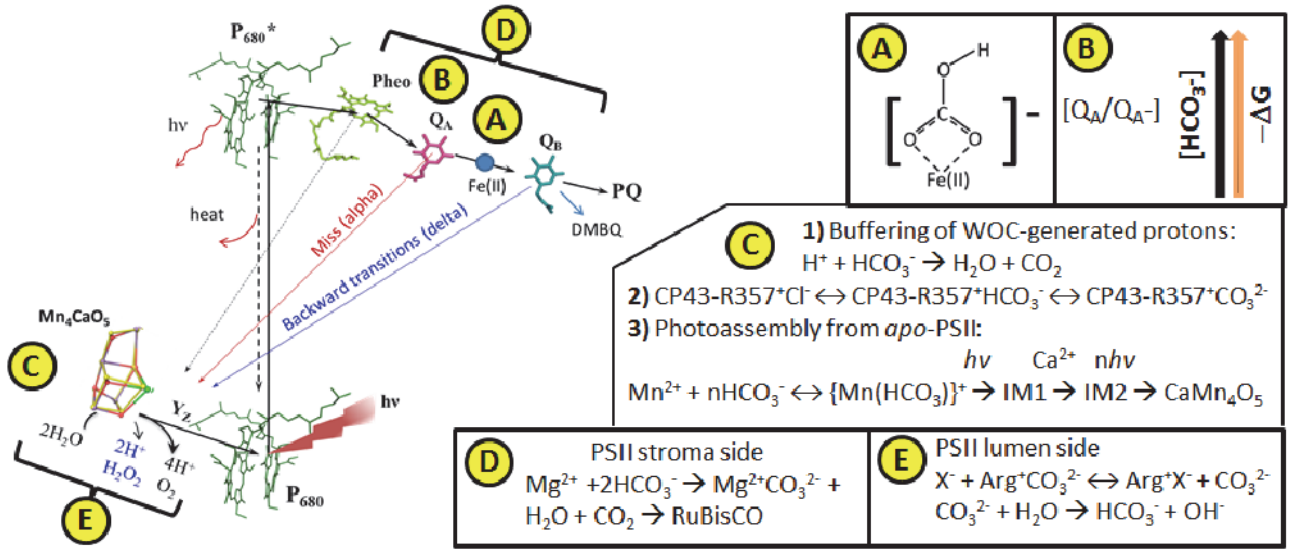

Scheme 1. Current map of HCO_3^- action sites within PSII involving electron and proton transfer steps, cofactor electrochemical potentials and photoassembly of the WOC. Stromal-side reactions: (A), (B), and (D); lumenal-side reactions: (C) and (E).

arginine with neutral serine exhibits a 50% decrease in (bi)carbonate-dependent O_2 evolution (Ananyev *et al.* 2005, Hwang *et al.* 2007). CP43-arginine357 was originally suggested to bind (bi)carbonate, reported in the 0.35 nm resolution PSII crystal structure by Ferreira *et al.* (2004), but not supported in later higher resolution structures by others (Shen 2015). An important feature of carbonate–guanidinium (Arg) ion pairing is the distinctively increased molar conductivity at high dilutions stemming from the strong basicity of liberated CO_3^{2-} which dissociates into OH^- and HCO_3^- (Scheme 1*C*, Eq. 2, 1*E*) (Khorobrykh *et al.* 2013). The extremely high conductance of the liberated OH^- in water *via* proton tautomerism is the main benefit of this mechanism relative to the minor contribution from spontaneous water dissociation. In this way, rapid neutralization of protons released at distant sites, potentially from the water oxidation site, can occur to the numerous carbonate–guanidinium sites throughout PSII. Light-driven changes in electrostatic forces or conformational changes accompanying S-state transitions may serve to liberate CO_3^{2-} from Arg to initiate this rapid proton neutralization mechanism.

Another function of the high (bi)carbonate buffering afforded by Arg and Lys residues in PSII is its postulated source of neutral CO_2 molecules for carbon fixation by Rubisco (Hillier *et al.* 2006). CO_2 is released during both proton neutralization (Scheme 1*C*, Eq. 1) and spontaneous dissociation (Scheme 1*D*), often termed carbonic anhydrase activity. The resulting neutral CO_2 molecule has a larger diffusion constant and lower energy barrier to cross membranes than do the charged forms.

The DIC buffer in the luminal space has been shown to be indispensable for photoassembly of the $CaMn_4O_5$ cluster from the free inorganic cofactors and apo-WOC–PSII complex during biogenesis and repair (Baranov *et al.* 2004, Dasgupta *et al.* 2008, Ananyev *et al.* 2017). Two roles have been identified for (bi)carbonate during photoassembly of the PSII–WOC. First, these anions pair with positively charged residues of apo-WOC–PSII resulting in electrostatic steering of Mn^{2+} to the apo-WOC site that accelerates the rate and increases the yield of recovery of O_2 evolution. Second, hyperfine coupling from ^{13}C-labeled bicarbonate shows that it coordinates to Mn^{2+} in forming the first photoassembly intermediate (Dasgupta *et al.* 2010), which electrochemically stabilizes photooxidation to Mn^{3+} and forms the binding site for the next Mn^{2+}.

Herein we apply a new method for more complete and selective removal of DIC to intact cells of *A. maxima* that combines two strategies: a (bi)carbonate-chelating agent (arginine) together with Mg^{2+} to induce release of CO_2 from bicarbonate (Scheme 1*D*). Key observations for intact cells are: (*1*) 99% of PSII charge separation and water-oxidation activity can be prevented in intact cells; (*2*) complete reconstitution of PSII activity by back titration with bicarbonate; (*3*) three distinguishable DIC action sites are revealed; and (*4*) comprehensive measurements of the electron transfer times for water oxidation (the WOC S-states), charge recombination, and Q_A^- reoxidation are reported. We identified a new role for DIC, distinct from previous reports, which is required for primary charge separation in the PSII reaction center and is revealed by inhibition of chlorophyll (Chl) variable fluorescence.

Materials and methods

Arthrospira (Spirulina) maxima (CS-328) was obtained from the Tasmanian CSIRO Collection of Living Microalgae and grown at 30°C in batch culture in 2.8-L Fernbach flasks containing 500 mL of standard Zarrouk's medium (Zarrouk 1966) (initial pH 9.5) supplemented with 200 mM $NaHCO_3$. Cultures were illuminated by cool fluorescent lamps in 12-h light/dark cycles. Light intensity was 16 μmol(photon) m^{-2} s^{-1}. Samples for experiments were taken in mid-exponential growth phase (three-day-old culture).

Removal of DIC: Treatment of *A. maxima* cells to remove DIC was examined using three reaction mixtures: a variant on the previously reported formate treatment used in almost all examinations of bicarbonate depletion in PSII to date (Govindjee and van Rensen 1993, Klimov *et al.* 1995, Brinkert *et al.* 2016) and two novel approaches reliant on arginine as the primary depleting agent. The goal was to minimize the remaining flash O_2 yield and maximize oxygen recovery after re-addition of HCO_3^- to the initial concentration.

Mixture #1	formate	Standard Zarrouk's medium without HCO_3^-, supplemented with 100 mM sodium formate	ACS grade; Fisher Scientific	pH 7.8
Mixture #2	NaCl+chelator	Standard Zarrouk's medium without HCO_3^-, supplemented with 400 mM NaCl, 10 mM L-arginine	USP grade; Amresco	pH 7.8
Mixture #3	$MgCl_2$+#2	Standard Zarrouk's medium without HCO_3^-, supplemented with 400 mM NaCl, 10 mM L-arginine; 100 mM $MgCl_2$	USP grade; Amresco	pH 7.15

All samples treated with a reaction mixture were washed four times with that reaction mixture. Between treatments, the supernatant was removed by centrifugation at 14,000 × *g* for 20 s each. All treatments were done under low light [<1 μmol(photon) m^{-2} s^{-1}] conditions. Prior to measurements, samples were incubated in total darkness for at least 1 h. For Mixture #3, the incubation time was 4 h. Alterations to incubation times are specified where made. The effectiveness of individual treatments is given in Table 1S (*supplement available online*).

Reconstitution with bicarbonate was carried out by washing DIC-depleted cultures twice in Zarrouk's medium supplemented with the desired amount of $NaHCO_3$. Between washes, supernatant was removed by centrifugation at 14,000 × *g* for 20 s. Washes were done under low light [<1 μmol(photon) m^{-2} s^{-1}] conditions and kept in darkness unless otherwise specified.

Measurement of flash O_2 by thin layer micro-cell/Clark electrode: O_2 production per flash in cells was measured in an aerobic "wet" chamber capable of regulating physiological conditions over the life of experiments, as previously described (Ananyev *et al.* 2016). Humidity, CO_2 and O_2 concentrations in the chamber were controlled. The membrane-bound Pt/Ir electrode has a sensitivity of about 1×10^{-15} mol(O_2) s^{-1} and time resolution of 100 ms. Flashes were generated using a 5-W light-emitting diode at wavelength 660 nm and light intensity of 32,000 μmol(photon) m^{-2} s^{-1}. The time required for a single turnover flash was determined to be 50 μs (Ananyev *et al.* 2016). A flash frequency of 0.5 Hz was used for all measurements.

Chl fluorescence measurements were taken using a home-built laser fast repetition rate (FRR) fluorometer with Peltier temperature-controlled cuvette previously described in Ananyev and Dismukes (2005). The variable Chl emission yield, F_v/F_m, was calculated from F_0 and F_m as $F_v = F_m - F_0$. Oscillations in F_v/F_m were produced using a GaAs laser that generated pulses of single-turnover flashes of 20 μs duration and 80,000 μmol(photon) m^{-2} s^{-1} intensity (equivalent photon flux as delivered for oxygen evolution). This fluorometer is capable of delivering saturating flashes at all frequencies examined.

The flash induced oscillations of O_2 yield and F_v/F_m were analyzed by model-dependent nonlinear least-squares fitting using an advanced WOC cycle model denoted VZAD, as described in prior work (Vinyard *et al.* 2013, Ananyev *et al.* 2016). VZAD accuracy was confirmed by root-mean-squares deviation of the theoretical fit to the experimental oscillation pattern.

To determine S-state decay lifetimes, a dark-acclimated culture was advanced to the desired state using single-turnover flashes, followed by dark incubation in this state, then rapidly advanced to oxygen evolution *via* further flashes (Babcock *et al.* 1989, Ananyev *et al.* 2016, Gates *et al.* 2016). The populations on any given flash were corrected using the WOC inefficiency parameters listed in Table 1.

S-state transition times (Si → Si+1) were measured from the change of F_v emission intensity using a train of flashes and the above FRR fluorometer. Samples were dark-adapted for 3 min to populate the dark-stable S-states, then exposed to a train of 1,000 "quarter-turnover" 5-μs flashes at 10-μs intervals (10-ms duration). Samples were subsequently incubated for 3 s in darkness to reoxidize the acceptor side of PSII while retaining scrambled S-states, after which another identical train of 1,000 flashes was applied. The fluorescence yield of the "scrambled" S-states was subtracted from that of the "dark-stable" S-states. Inflections in the plot of this difference represent transitions between redox states on the donor or acceptor side of PSII that cause different F_v intensities.

The reoxidation time of Q_A^- was measured using the same fluorometer. A single saturating flash was delivered to a dark-incubated culture sample to fully reduce Q_A, after which the sample was left in darkness for a variable time before a second saturating flash was then delivered. The F_v fluorescence amplitude of the first flash represents the maximal photoreduction of the Q_A population. The difference between F_m of the first flash and F_0 of the second flash gives the population of oxidized Q_A remaining after the variable time. $(F_m1 - F_02)/(F_m1 - F_01)$ therefore equals percent reoxidation of Q_A. This method differs from the pulse amplitude modulation method (Kolber *et al.* 1998) by not using subsaturating probe flashes which induce secondary charge separation events and contaminate results.

Results

Optimization of treatment by different reaction mixtures: The purpose of the extraction experiments was to determine the effectiveness of three methods for removal of DIC and their reversibility upon reconstitution with $NaHCO_3$. Table 1S lists the content of the extraction mixtures and protocols. All samples were in equilibrium with atmospheric CO_2. Treated culture samples were investigated for PSII operation *via* FRR fluorescence at 100 Hz (Fig. 1*A*) and flash oxygen yield at 0.5 Hz (Fig. 1*C*), representing standard measurement conditions for each technique. For all treatments, the decline in oxygen yield (PSII linear electron flow) was at least one order of magnitude greater than the corresponding decrease in F_v/F_m (PSII primary charge separation). Extraction with Mixtures 1 (formate), 2 (NaCl+chelator), and 3 ($MgCl_2$+ NaCl+chelator) inhibited PSII activity with increasing effectiveness: the percentage of F_v/F_m retained was 83, 74, and 53%, respectively, while the steady-state

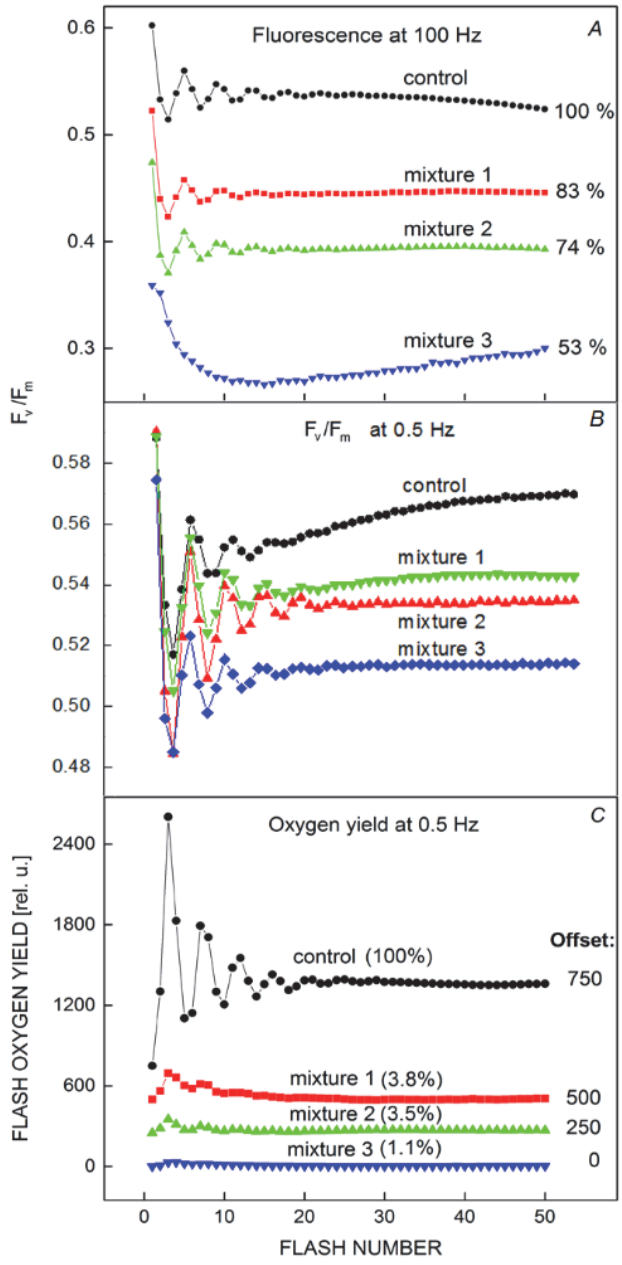

Fig. 1. Effect of different extraction methods for DIC from *Arthrospira maxima* cells *in vivo* on F_v/F_m at (*A*) 100 Hz and (*B*) 0.5 Hz flash rate. (*C*) Effect of same treatments on flash oxygen yield (relative units, samples of equal cell density) at 0.5 Hz. Curves shifted to avoid overlap (*see* Fig. 1S for improved resolution). Average percent activity given at right of each train in (*A*) and above traces in (*C*). All kinetics shown are the average of 20 flash trains.

yield of O_2 evolution (Yss) retained was 3.8, 3.5, and 1.1%, respectively (*see* Table 1S). Mixture 3 produced the deepest extraction of DIC, as judged by Yss and a complete loss of oscillations in F_v/F_m, indicating full shutdown of the WOC cycle. Table 1 gives fits of the O_2 oscillations to the WOC cycle model (VZAD).

In order to test if the extraction methods were reversible, treated culture samples were resupplied with native concentrations (200 mM) of $NaHCO_3$ and incubated for two hours under soft light (Fig. 2, also see Fig. 2S, *supplement available online*). After treatment with each reaction mixture, approximately full return of Yss was observed (Table 1S). In the case of Mixture 2, the oxygen yield increased above the control level to 110% and oscillations were fully restored, indicating photoassembly (photoactivation) of some inactive PSII centers. Samples treated with the Mixture 3 recovered to 96% of initial Yss, but oscillation quality visibly decreased, indicating altered population of S-states in the dark. The WOC cycle inefficiency parameters derived from fitting to the VZAD model are given in Table 1.

DIC influence on DMBQ-dependent O_2 production: Prior experiments have shown that the electron acceptor DMBQ diminishes both oxygen evolution yield and WOC cycle efficiency in *A. maxima,* in contrast to its usual beneficial effect on all other phototrophs (Ananyev *et al.* 2016). To determine the extent to which this unusual loss of activity is influenced by DIC, DIC-depleted samples were supplemented with DMBQ and flash oxygen yields measured (Fig. 3*B*). In samples treated with Mixture 2, DMBQ insignificantly influenced only the dark S-state populations. However, change in Yss improved oscillation quality (hence, influencing only the dark S-state populations). However, more thorough depletion of DIC with Mixture 3 resulted in a beneficial effect of DMBQ addition, causing more than 50% increase in Yss, oscillations more pronounced in amplitude and extended further along the flash train. This shows that thorough DIC extraction (>96% of loss of oxygen yield) results in a positive influence of DMBQ addition on activity.

To examine time-dependent consequences of DIC depletion, Chl fluorescence kinetics were measured after a shorter treatment with Mixture 3, which allowed retention of some residual DIC (Fig. 4). Under DIC-repleted conditions, an activation of F_v/F_m is observed during the flash train, when using slow flash rate (0.5 Hz), that is not visible at high flash rate (100 Hz) (Fig. 4*A*) or without DIC present (Fig. 4*B*). Under both conditions, Yss is markedly higher at lower frequency. The higher Yss is normal, as the acceptor side clears faster by two orders of magnitude compared to S-state recombination. The higher flash frequency suppresses detection of recombination and the oscillation amplitudes are thus larger. However, under DIC-depleted conditions, the gap between Yss at the two flash frequencies is three times as large as under repleted conditions.

Influence of DIC on S-state transition times: To investigate any S-state specific influence of DIC, the S-state transition times were measured from their influence on Chl variable fluorescence. F_m measurements were carried out at several temperatures in order to constrain DIC diffusion and to investigate possible correlation with the thermal-

Table 1. WOC cycle parameters from fits of the flash oxygen yields at 0.5 Hz using the VZAD model. Recovered samples were treated with 200 mM $NaHCO_3$ after DIC depletion.

	Control	Fig. 2*A*, recovered from Mixture 2	Fig. 2*B*, recovered from Mixture 3	Fig. 3*A*, no DIC	Fig. 3*A*, no DIC + DMBQ
Alpha	0.171	0.150	0.222	0.174	0.123
Beta	0.021	0.028	0.017	0.0223	0.036
Delta	0	0	0	0	0
Epsilon	0.041	0.016	0.038	0.039	0.0087
S0	0	0.0316	0	0	0.321
S1	0.858	0.817	0.919	0.840	0.594
S2	0.142	0.152	0.081	0.160	0.085
S3	0	0	0	0	0
Period	4.44	4.37	4.78	4.50	4.28

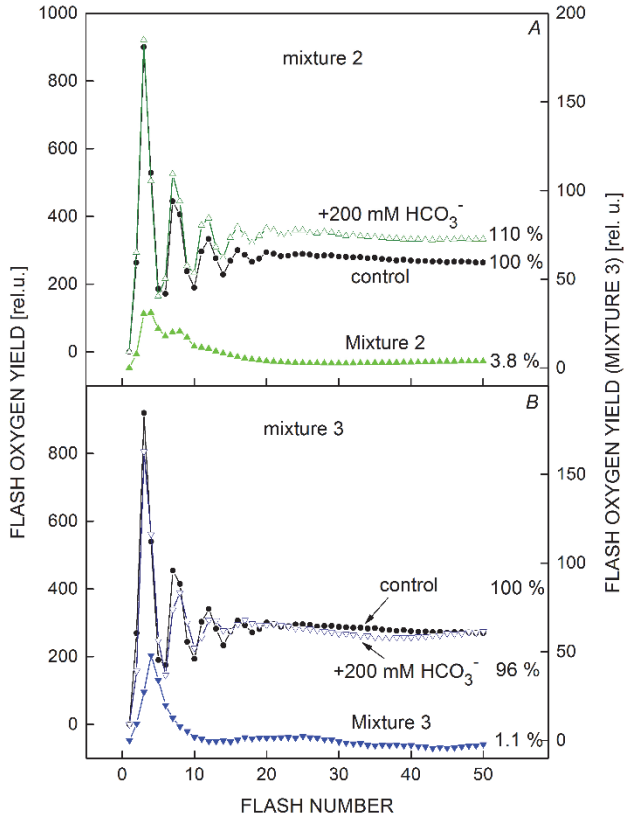

Fig. 2. Recovery of flash oxygen evolution over 2 h under white light of 9 µmol(photon) m^{-2} s^{-1} from soft fluorescent bulbs after DIC removal by (*A*) Mixture 2; and (*B*) Mixture 3. Control culture contains 200 mM DIC. All measurements were taken at 0.5 Hz flash frequency using samples of equivalent biomass as determined by OD730. Kinetics of recovery are given in Fig. 2S.

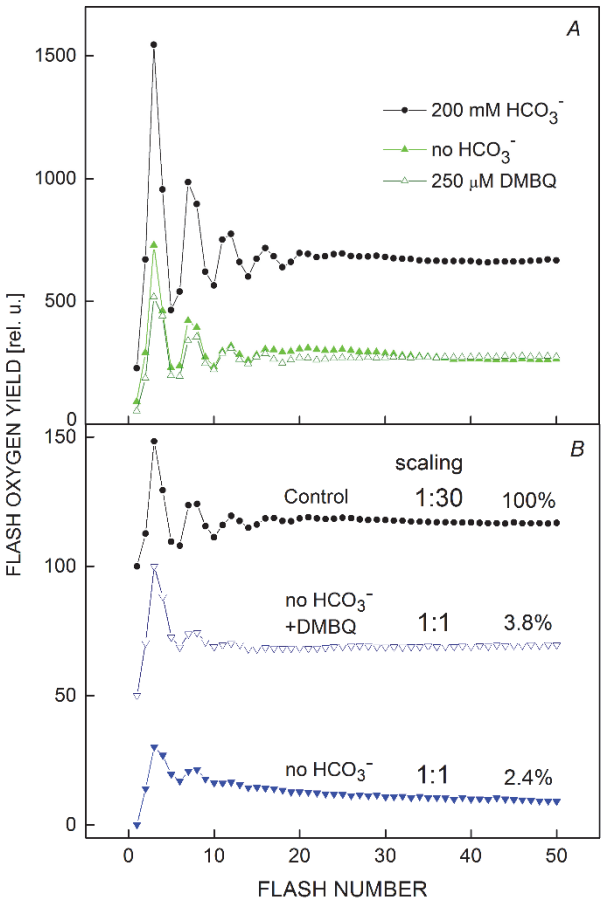

Fig. 3. Influence of 2,5-dimethylbenzoquinone (DMBQ) on flash O_2 production from *Arthrospira maxima* cells that have been DIC-depleted using (*A*) Mixture 2 and (*B*) Mixture 3. In (*B*), control was scaled down 30-fold for comparison and control and +DMBQ were offset by 100 and 50 relative units, respectively, for clarity. Control culture contains 200 mM DIC. All measurements were taken at 0.5 Hz flash frequency.

dependent phase of F_m (the J step in the induction of F_m, called the Kautsky induction curve), which may correlate with the terminal step of oxygen release (Stirbet and Govindjee 2011.

Fig. 5*A* shows the dark-scrambled F_m difference kinetics *vs*. time from 10 to 10,000 µs measured at 25°C. Data are plotted logarithmically for the control sample grown in 200 mM HCO_3 and an identical sample treated with Mixture 2. This 10-ms interval is theoretically sufficient time to induce 2–3 full WOC cycles. The F_m1 trace was taken after 3 min in the dark and corresponds to "dark" S-state population (obtained from the VZAD model

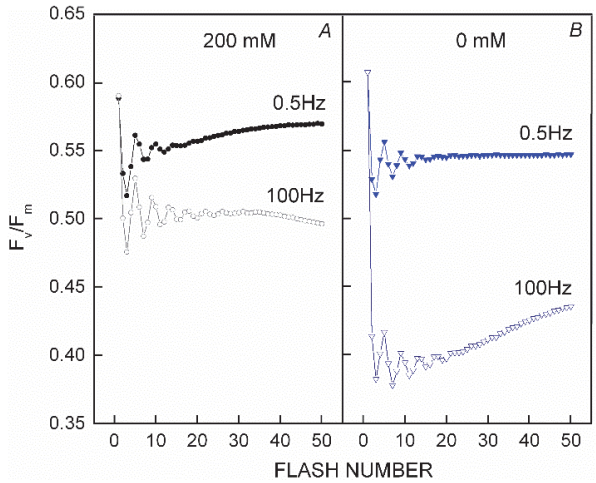

Fig. 4. Effect of (*A*) 200 mM and (*B*) 0 mM HCO_3^- on F_v/F_m kinetics at low (0.5 Hz) and high (100 Hz) flash frequencies. Mixture 3 was used for DIC depletion; samples were pre-incubated in darkness for 30 min.

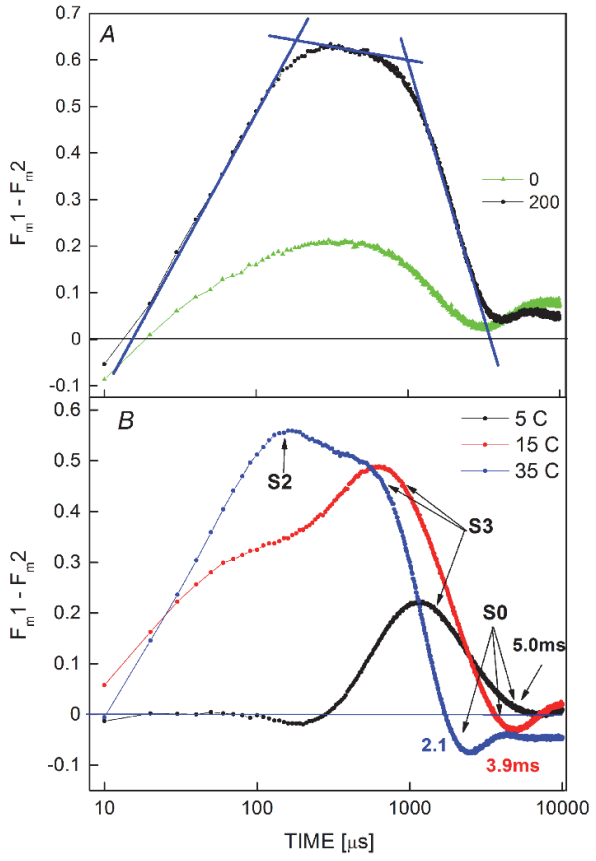

Fig. 5. Fluorometric measurements of S-state transition times using 1,000 "quarter-turnover" 5-µs flashes at 10-µs intervals, from whole cells of *Arthrospira maxima*. The F_m1(dark S) – F_m2(scrambled S) difference in emission yield from: (*A*) DIC-depleted by Mixture 2 and DIC-replete in 200 mM NaHCO3 at 25°C, and (*B*) DIC-repleted conditions at 5, 15, and 35°C. The logarithmic plot format converts single exponential changes into linear regions, shown as straight lines. Data shown are the average of 24 replicates.

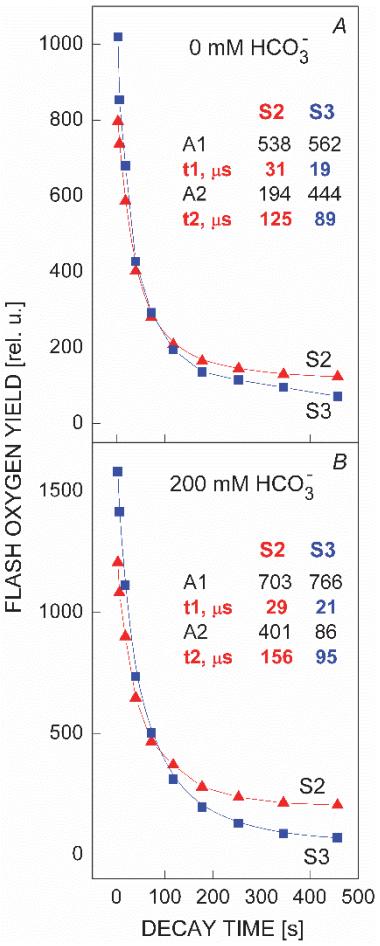

Fig. 6. Dependence of lifetime of S2 and S3 states (charge recombination time constants) on the DIC concentration in *Arthrospira maxima* cells measured by flash O_2 yield. Insets show fitting parameters from biexponential decay fits to data. (*A*) DIC-depleted (by Mixture 2); and (*B*) control culture.

fit of the flash O_2 data; *see* Table 1). The F_m2 trace was taken 3 s after the dark trace, which is short compared to decay of S2 and S3 (Fig. 6) and so is labelled as "scrambled" populations. Removal of DIC reduces the differential fluorescence amplitude (proportional to the number of PSIIs that can do charge separation) by approximately two thirds and broadens the peak features. When additional $NaHCO_3$ is added to the media to 1 M, approaching the saturation limit found in *A. maxima*'s native environment, the maximum F_m difference amplitude increases by 16% (from 0.69 to 0.8 units; Fig. 3S*A*, *supplement available online*). Relative to this value, the DIC-depleted sample amplitude is four-fold lower, which is consistent with the foregoing DIC-depletion data showing DIC-depletion reduces F_v/F_m only when a rapid flash rate is used (Fig. 4).

Three regions are resolved in the first 2-ms interval shown in Fig. 5*A*. The logarithmic plot format converts single exponential changes into linear regions and is convenient for deconvolution, as shown by the straight

lines. The fluorescence rises from the initial dark state, mainly S1 (Table 1), linearly in log(time) corresponding to the induction of the S2 state (196 μs), followed by a plateau corresponding to formation of S3 (1.1 ms), followed by a linear decay to a minimum, corresponding to the formation of S0 (3.5 ms). The individual S-state transition times are listed in Table 2S (*supplement available online*). The corresponding transition times in μs for the DIC depleted sample are (S1'→S2') 200, (S2'→S3') 530, and (S3'→S0') 2,300, with a total transit time of 3.0 ms.

To aid in deconvoluting the changes, we showed in Fig. 5*B* two previously established general effects of temperature on the WOC cycle transitions: (*1*) at the lowest temperature (5°C), where the WOC cycle is blocked from advancing past S3 in *A. maxima*, the characteristic collapse of the S2 peak as this transition slows and the initial dark populations change; (*2*) as the temperature increases to 15°C the full WOC cycle occurs within 3.9 ms and 35°C it accelerates to 2.1 ms.

S2 and S3 state lifetimes: To study the effect of DIC on the lifetimes of the S2 and S3 states, we measured the loss of flash oxygen yield over a variable dark period following population of S2 and S3 by one and two pre-flashes, respectively, using a previously described method (Rutherford *et al.* 1984, Ananyev *et al.* 2016, Gates *et al.* 2016). In addition to the previously demonstrated negative effect of DIC depletion on oxygen yield, several shifts in decay kinetics were observed (Fig. 6). After DIC depletion the bi-exponential fits of S2 population decay showed approximately 20–25% slower decay constants but the quicker feature became more dominant. Minimal change in the S3 decay time constants was seen upon DIC depletion, and the quicker feature became slightly more dominant. The dark populations of the S-states after full decay of S2 and S3 were identical whether observed by flash oxygen or Chl fluorescence measurements (Fig. 4, Table 1).

Q_A^- reoxidation time: As the role of DIC at the non-heme iron/Q_A site is well-known, we attempted to investigate DIC depletion on the yield of Q_A^- and its reoxidation kinetics. Fig. 4S (*supplement available online*) shows the reoxidation rate under DIC-repleted conditions in *A. maxima* is exceptionally slow, but in the absence of DIC, the fast component of reoxidation takes about 35% less time on average and is responsible for a slightly larger fraction of overall decay. As expected, no Q_A^- is retained beyond the measurement time of 6 ms (full reoxidation occurs).

Discussion

Sites of DIC removal: The three reaction mixtures used for DIC depletion were selected to remove (bi)carbonate bound to PSII with varying affinities. A loss of PSII activity and restoration upon reconstitution was observed for all three treatments. Mixture 1 (formate) is a well-known inhibitor of bicarbonate stimulation of PSII-dependent O_2 evolution, "the bicarbonate effect" (Stemler 1980, Brinkert *et al.* 2016). This is the weakest of the three DIC depletion treatments. Using FRR fluorometry and flash O_2 yield as in Figs. 1 and 4, we were able to further elucidate its function. The 96% decrease in O_2 yield (measured at 0.5 Hz flash rate) without corresponding loss in F_v/F_m or their oscillations (96% retained at 0.5 Hz, 83% retained at 100 Hz) indicates that essentially all PSII–WOCs remain fully active in charge separation between P680 and Q_A at low flash rates and progressively lose activity at increasing flash rates. Increasing flash rates correspond to higher continuous light intensities used in historical measurements. While period-four oscillations in F_v/F_m are retained in proportion to their steady-state values, O_2 evolution is nearly zero, 3.8% at flash rate 0.5 Hz. The retention of F_v/F_m steady-state level and period-four oscillation amplitude at low flash rate in DIC-depleted samples indicates that primary charge separation and coupling to the water-oxidation cycle are unaffected. At higher flash rates, the steady-state F_v/F_m decreases, owing to decline in F_m, while the oscillation amplitude is unaffected or even improves at 100 Hz (Fig. 4), indicating that the electron acceptor capacity is reduced as the flash rate increases [size of the plastoquinone (PQ) pool or its kinetics of filling]. The major loss of F_v/F_m occurs on flash #2, indicating that the reoxidation of Q_A^- is rate-limiting ($Q_A^-Q_B \rightarrow Q_AQ_B^-$). This interpretation is consistent with the consensus view that formate treatment slows this step by removal of bicarbonate from coordination to the non-heme iron (Scheme 1*A*). Removal of (bi)carbonate from this site *in vitro* was shown to shift the electrochemical reduction potential of the Q_A/Q_A^- couple by +75 mV *in vitro* (Brinkert *et al.* 2016), though the location of the site(s) involved was not established. This shift was shown to protect PSII from photodamage *in vitro* by reducing the yield of singlet oxygen formation ($^1O_2$). These authors postulated that redox tuning of Q_A/Q_A^- could be necessary for *in vivo* photoprotection. Specifically, the authors suggest that population of Q_A^- (as occurs when Q_B and the PQH_2 pool are reduced) could enhance HCO_3^- loss, resulting in Q_A redox tuning *in vivo* and lower $^1O_2$ formation.

The nearly complete loss of O_2 evolution was observed at low flash rates following formate treatment which occurs without loss of period-four oscillations in F_v/F_m. Thus the PSII–WOC works fine and another DIC site must be responsible. The absence of O_2 detection may stem from various mechanisms: 1) uptake of O_2 by increased cellular respiration, 2) increased consumption of PSII-generated O_2 by the Mehler reaction (PSI-dependent

reduction of O_2), or 3) possibly by an altered WOC cycle that produces two H_2O_2 molecules rather than O_2 (chemically least likely). The cause for loss of O_2 evolution is a subject for future research.

Deeper depletion of DIC sites: Compared to formate treatment, Mixture 2 (NaCl + chelator) was developed to remove more aggressively (bi)carbonate bound to arginine residues in PSII by chelating the (bi)carbonate ion to the guanidinium side chain of added arginine. It results in a lower steady-state yield of F_v/F_m (74% at 100 Hz) with oscillations somewhat clearer (extending to higher flash number), and the O_2 yield is eliminated to the same extent as formate treatment (3.5%). Mixture 2 seems to accomplish the same outcome, but with greater depletion of DIC from PSII centers.

There are 102 arginine residues in PSII core complexes of *A. maxima*, the majority located near the lumenal and stromal surfaces where they can exchange (bi)carbonate ligands (Scheme 2). The guanidinium cation is an especially good chelator of HCO_3^- and CO_3^{2-}, owing to the combination of bidentate H-bonding and ion-pairing interactions (Scheme 2). Arginine/carbonate ion pairs are frequently found in the crystal structures of proteins (Ippolito *et al.* 1990). The free energy of guanidinium–carbonate ion pair formation is –16 kJ mol^{-1} in dimethyl sulfoxide/water (80:20) (Armstrong *et al.* 2016). This value corresponds to a formation constant of 500 M^{-1}. (Bi)carbonate anions have even stronger affinity for guanidinium cations in more hydrophobic environments such as the interior of membrane-bound proteins. (Bi)carbonate has even stronger affinity for arginine than for guanidinium, which enables Arg to take up DIC from solution into cells. An important feature of (bi)carbonate–guanidinium ion pairing is the distinctively increased molar conductivity at high dilutions (Hunger *et al.* 2013). This results from dissociation of CO_3^{2-} from the ion pair, thus liberating a strong base that spontaneously hydrolyzes to form OH^- and HCO_3^-. The well-known anomalously high conductivity of hydroxide and hydronium ion occurs because neither relies on bulk diffusion through water, but rather proton tautomerism of the solvent water. We propose that the numerous arginines found on the luminal surface of PSII use this mechanism to achieve unusually rapid proton neutralization by liberating CO_3^{2-} during water oxidation in hypercarbonate-requiring strains like *A. maxima* [PSII–WOC turnover is 4–5 fold faster in *A. maxima* than other conventional oxygenic phototrophs (Khorobrykh *et al.* 2013)]. To dissociate carbonate from arginine, other anions such as Cl^- are likely candidates (Scheme 2).

Mixture 3 ($MgCl_2$ + chelator) is made by adding $MgCl_2$ to Mixture 2. It was developed to include the possibility of removing CO_2 by shifting the equilibrium in the reaction: $Mg^{2+} + 2HCO_3^- \rightarrow Mg^{2+}CO_3^{2-} + CO_2 + H_2O$ (Scheme 1*D*) to favor formation of volatile CO_2 *via* ion-pairing of Mg^{2+} and carbonate. This treatment causes a complete loss of both O_2 evolution and oscillations in F_v/F_m (at high frequency), and greatly reduces the high yield of the first flash F_v/F_m characteristic of a fully oxidized Q_A population (Ananyev and Dismukes 2005). Mixture 3 is therefore able to remove DIC from an additional site(s) resulting in loss of both donor side reactions that drive water oxidation and the acceptor side electron/proton transport. The acceptor-side influence is further seen in Fig. S4, where of the three treatments only Mixture 3 caused a significant change

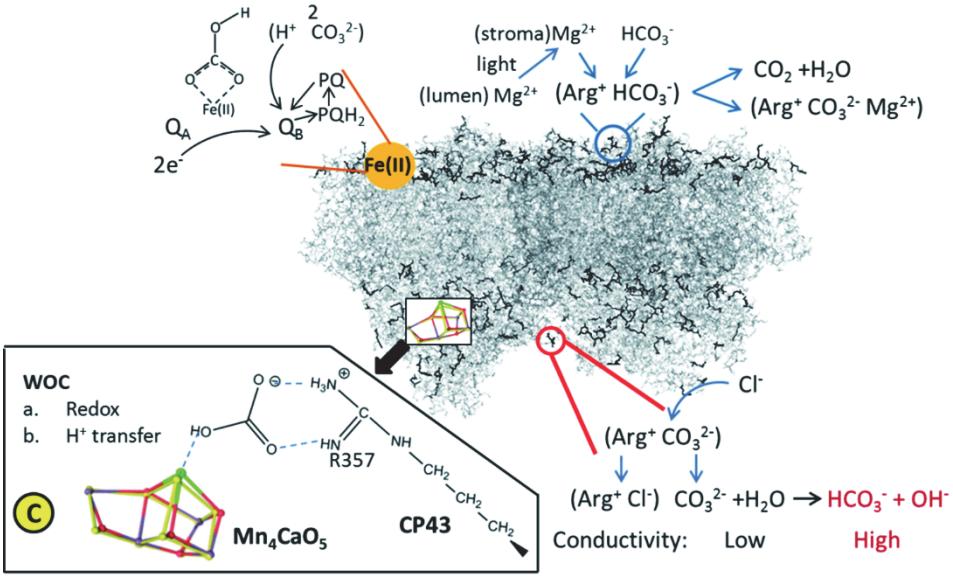

Scheme 2. Proposed ligand-ligand exchange in PSII at multiple sites, including the WOC region, the non-heme iron, and the solvent-exposed arginine residues. Arginine residues in PSII dimer depicted in black (102 in total, located on both lumenal and stromal sides). Proposed functions of (bi)carbonate shown for WOC-region, Fe(II)/Q_A, general lumenal and general stromal sites.

in Q_A^- reoxidation kinetics. Magnesium is transported from the lumen into the stroma across the thylakoid membrane during photosynthetic electron transport (PET), where it is known to activate the CO_2 fixation activity of Rubisco (Kuriata *et al.* 2014). We postulate that in addition to this well-known activation of Rubisco, PET-elevated magnesium in the stroma enables synchronized conversion of bicarbonate into carbon dioxide by the reaction: $HCO_3^- + Mg^{2+} + \text{stromal-Arg}^+(HCO_3^-) \rightarrow CO_2 + \text{Arg}^+(CO_3^-)Mg^{2+}$ (Scheme 2). The liberated CO_2 is then in the correct chemical form that Rubisco can use for carboxylation.

Flash rate dependence of DIC-depletion effects: Unlike the case of complete DIC depletion, the first flash F_v/F_m yield is not decreased when the treatment with Mixture 3 is shortened to avoid removal of the most tightly bound DIC associated with the donor side (Fig. 4). Thus, the donor side works and Q_A can be maximally photoreduced. However, at 100 Hz flash rate the second flash occurs 10 ms later and the yield is greatly suppressed, indicating that Q_A^- reoxidation by Q_B is slowed or blocked. Accordingly, we attribute the DIC site that blocks PET *in vivo* to be either the non-heme iron site, which has been shown to lose bicarbonate *in vitro* (Brinkert *et al.* 2016), or alternatively, a site that blocks the transfer of protons to Q_B (van Rensen *et al.* 1988).

Remediation of DIC-depletion effects: Although all three treatments are reversible upon reconstitution with $NaHCO_3$, there are some differences in performance of reactivated PSII–WOCs evident from the quality of oscillations. This is most clearly revealed by the WOC cycle parameters obtained from minimized-error fits to the VZAD model and summarized in Table 1 (Vinyard *et al.* 2013). Readdition of $NaHCO_3$ after treatment with Mixture 2 resulted in lower misses (alpha) and fewer inactivations (epsilon), indicating the restored PSII–WOC is operating somewhat more efficiently than the control culture. By contrast, readdition after treatment with Mixture 3 sharply increased misses, resulting in a lengthening of the cycle period by 0.34 to 4.78. These changes indicate that the 4-h extraction period using Mixture 3 can cause damage that is not readily reversed by $NaHCO_3$.

Donor-side effect of DIC on S-state transitions: The most obvious effect of DIC depletion from the acceptor side DIC site (*i.e.*, using Mixture 2) is the 3-fold loss of amplitude of $F_m1 - F_m2$, arising from fewer centers advancing through the cycle. After normalizing the two curves in Fig. 5*A* to the same peak amplitude (*see* Fig. 3S*B*, *supplement available online*) the slopes can provide an estimate of the relative changes in the individual S-state transition times, assuming the S-state dependent F_v quantum yield does not change with/without DIC (this is unknown and may be invalid). The most prominent effect is the shorter overall transit time to reach the minimum (3.0 ms *vs*. 3.5 ms at 25 °C). The minimum corresponds to transit through the full cycle with formation of the S0 state in the DIC-replete sample. For the DIC-depleted sample, we attribute the rise and fall of the $F_m1 - F_m2$ signal to the same S-state transitions but with the lower yield. If this assignment is correct, at 25°C, the S1'→ S2' is unchanged at 200 μs, while S2'→S3'at 530 μs is 35% faster, and S3' →S0' at 2,250 μs is 10% faster.

Distinguishing functions and sites of DIC activity: DIC removal with Mixture 2 accesses lower-affinity sites, while Mixture 3 accesses these and a higher affinity site on the donor side that shuts down water oxidation. The lower affinity sites include both the classic acceptor-side site at the non-heme iron and presumably multiple other potential (bi)carbonate sites associated with the 102 arginine residues. These sites are still conspicuously occupied in the active PSIIs even after massive loss of oxygen yield, as evident by the retention of high first-flash fluorescence yields and visible oscillations in both oximetric and fluorometric measurements (Figs. 1–3). However, they work efficiently only at low flash rates (low light flux) where residual DIC or alternative pathways independent of DIC can function. We can posit that this site is one or more of the 102 solvent-accessible arginines within PSII. This "arginine network" represents a large potential DIC reservoir which, under *A. maxima*'s native conditions, would be expected to play multiple roles: a structural role, a role for HCO_3^- and CO_3^{2-} as proton acceptors on the luminal surface, and a role as CO_2 source on the stromal surface. These roles and the chemical mechanism by which they act are summarized in Scheme 2 and described above. As light is necessary to reverse the depletion at these sites, light-driven proton gradient or ATP production is required to transport bicarbonate to the site(s) of interest.

The donor-side function of DIC may be linked to the proton-removal process attributed to chloride. In that process, the S1–S2 transition, on which no protons are released, is unaffected by chloride removal (Wincencjusz *et al.* 1997), but the S2–S3 and S3–S4–S0 transitions are delayed. In DIC-depleted samples (Fig. 5*A*), most of the fluorescence yield is lost, but those centers, which remain active, have faster transitions through these S-states. We posit that the site of DIC function on the donor side is CP43-R357 (Ananyev *et al.* 2005). Furthermore, from this site, (bi)carbonate would be perfectly positioned to modulate the position of calcium within the WOC (Zhang *et al.* 2002), and in turn the redox potential of the WOC and individual S-states. The redox tuning effect of Ca^{2+} has been previously demonstrated (Vogt *et al.* 2015, Capone *et al.* 2016, Gates *et al.* 2016), and the effects of DIC removal are consistent with a reshaping effect on the S2 structure of the WOC (Lubitz *et al.* 2014, Askerka *et al.* 2015, Capone *et al.* 2016). Further support for this site comes from the lack of peroxide detected under partial depletion of DIC. This is the highest-affinity site, and loss of functionality at this site is known to induce peroxide

evolution [which is a further indicator of a reshaped S2 structure (Ananyev *et al.* 2005, Gates *et al.* 2016)]. We posit that this site is not occupied by DIC in high-resolution crystal structures because the treatment conditions are comparably harsh compared to our own DIC removal methods, using extreme concentrations of chloride (Shen 2015). One notable difference is that crystallization techniques involve first removing the small lumenal subunits of PSII, which facilitates diffusion of small molecules to/from the WOC pocket and removes a substantial number of arginines which might otherwise mediate the stress of DIC removal. It is likely that under these conditions, the local DIC affinity at CP43-R357 becomes lower than that at the non-heme iron site.

Conclusions: To elucidate the multiple roles of (bi)carbonate in PSII, we developed two new methods for DIC depletion capable of inhibiting oxygen evolution activity down to 1%, all of which were fully reversible by readdition of DIC and light. These techniques will allow further investigation of the role of DIC *in vivo* and may be applied to other species. DIC depletion was found to cause complete inactivation of PSII fluorescence prior to loss of either Q_A or WOC functionality. The previously observed detrimental effect of DMBQ in *A. maxima* was localized to the donor side, while the positive acceptor-side effect was shown to be dependent on DIC availability at the non-heme iron site. Depletion at the non-heme iron site was shown to facilitate forward electron transfer. The relative binding affinities of three distinct DIC sites were established to be WOC region > non-heme iron > unknown bulk inactivation site, though certain DIC-depleting agents were found to act with varying specificity for each site. We attribute the role at the donor side to free energy stabilization through structural modulation of the WOC *via* interaction at a site between CP43-R357 and Ca^{2+} in the WOC.

References

Ananyev G., Dismukes G.C.: How fast can Photosystem II split water? Kinetic performance at high and low frequencies. – Photosynth. Res. **84**: 355-365, 2005.

Ananyev G., Gates C., Dismukes G.C.: The oxygen quantum yield in diverse algae and cyanobacteria is controlled by partitioning of flux between linear and cyclic electron flow within photosystem II. – BBA-Bioenergetics **1857**: 1380-1391, 2016.

Ananyev G., Gates C., Dismukes G.C.: Biogenesis and assembly of the $CaMn_4O_5$ core of photosynthetic water oxidases and inorganic mutants. – In: Scott R. (ed.): Metalloprotein Active Site Assembly. John Wiley & Sons, Chichester 2017.

Ananyev G., Nguyen T., Putnam-Evans C., Dismukes G.C.: Mutagenesis of CP43-arginine-357 to serine reveals new evidence for (bi) carbonate functioning in the water oxidizing complex of photosystem II. – Photoch. Photobio. Sci. **4**: 991-998, 2005.

Armstrong C.T., Mason P.E., Anderson J.R., Dempsey C.E.: Arginine side chain interactions and the role of arginine as a gating charge carrier in voltage sensitive ion channels. – Sci. Rep. **6**: 21759**,** 2016.

Askerka M., Vinyard D.J., Brudvig G.W., Batista V.S.: NH_3 Binding to the S2 state of the O_2-evolving complex of photosystem II: Analogue to H_2O binding during the S2→ S3 transition. – Biochemistry **54**: 5783-5786, 2015.

Babcock G.T., Barry B.A., Debus R.J. *et al.*: Water oxidation in photosystem II: from radical chemistry to multielectron chemistry. – Biochemistry **28**: 9557-9565, 1989.

Baranov S., Tyryshkin A., Katz D. *et al.*: Bicarbonate is a native cofactor for assembly of the manganese cluster of the photosynthetic water oxidizing complex. Kinetics of reconstitution of O_2 evolution by photoactivation. – Biochemistry **43**: 2070-2079, 2004.

Brinkert K., De Causmaecker S., Krieger-Liszkay A. *et al.*: Bicarbonate-induced redox tuning in photosystem II for regulation and protection. – P. Natl. Acad. Sci. USA **113**: 12144-12149, 2016.

Capone M., Narzi D., Bovi D., Guidoni L.: Mechanism of water delivery to the active site of photosystem II along the S2 to S3 transition. – J. Phys. Chem. Lett. **7**: 592-596, 2016.

Carrieri D., Ananyev G., Brown T., Dismukes G.C.: *In vivo* bicarbonate requirement for water oxidation by photosystem II in the hypercarbonate-requiring cyanobacterium *Arthrospira maxima*. – J. Inorg. Biochem. **101**: 1865-1874, 2007.

Clausen J., Beckmann K., Junge W., Messinger J.: Evidence that bicarbonate is not the substrate in photosynthetic oxygen evolution. – Plant Physiol. **139**: 1444-1450, 2005.

Dasgupta J., Ananyev G.M., Dismukes G.C.: Photoassembly of the water-oxidizing complex in photosystem II. – Coordin. Chem. Rev. **252**: 347-360, 2008.

Dasgupta J., Tyryshkin A.M., Baranov S.V., Dismukes G.C.: Bicarbonate coordinates to Mn3+ during photo-assembly of the catalytic Mn4Ca core of photosynthetic water oxidation: EPR characterization. – Appl. Magn. Reson. **37**: 137-150, 2010.

Diner B.A., Petrouleas V., Wendoloski J.J.: The iron-quinone electron-acceptor complex of photosystem II. – Physiol. Plantarum **81**: 423-436, 1991.

Drake B.G., Gonzàlez-Meler M.A., Long S.P.: More efficient plants: a consequence of rising atmospheric CO_2? – Annu. Rev. Plant Phys. **48**: 609-639, 1997.

Ferreira K.N., Iverson T.M., Maghlaoui K. *et al.*: Architecture of the photosynthetic oxygen-evolving center. – Science **303**: 1831-1838, 2004.

Gates C., Ananyev G., Dismukes G.C.: The strontium inorganic mutant of the water oxidizing center ($CaMn_4O_5$) of PSII improves WOC efficiency but slows electron flux through the terminal acceptors. – BBA-Bioenergetics **1857**: 1550-1560, 2016.

Govindjee, van Rensen J.: Photosystem II reaction centers and bicarbonate. – In: Deisenhofer j. (ed.): Photosynthetic Reaction Centers. Pp. 357-389, Academic Press, San Diego 1993.

Hillier W., McConnell I., Badger M.R. *et al.*: Quantitative assessment of intrinsic carbonic anhydrase activity and the capacity for bicarbonate oxidation in photosystem II. – Biochemistry **45**: 2094-2102, 2006.

Hunger J., Neueder R., Buchner R., Apelblat A.: A conductance study of guanidinium chloride, thiocyanate, sulfate, and carbonate in dilute aqueous solutions: ion-association and carbonate hydrolysis effects. – J. Phys. Chem. B **117**: 615-622, 2013.

Hwang H.J., Dilbeck P., Debus R.J., Burnap R.L.: Mutation of

arginine 357 of the CP43 protein of photosystem II severely impairs the catalytic S-state cycle of the H_2O oxidation complex. – Biochemistry **46**: 11987-11997, 2007.

Ippolito J.A., Alexander R.S., Christianson D.W.: Hydrogen bond stereochemistry in protein structure and function. – J. Mol. Biol. **215**: 457-471, 1990.

Khorobrykh A., Dasgupta J., Kolling D.R. *et al.*: Evolutionary origins of the photosynthetic water oxidation cluster: bicarbonate permits Mn^{2+} photo-oxidation by anoxygenic bacterial reaction centers. – Chem. Bio. Chem. **14**: 1725-1731, 2013.

Klimov V.V., Allakhverdiev S.I., Feyziev Y.M., Baranov S.V.: Bicarbonate requirement for the donor side of photosystem II. – FEBS Lett. **363**: 251-255, 1995.

Klimov V., Baranov S.: Bicarbonate requirement for the water-oxidizing complex of photosystem II. – BBA-Bioenergetics **1503**: 187-196, 2001.

Kolber Z.S., Prášil O., Falkowski P.G.: Measurements of variable chlorophyll fluorescence using fast repetition rate techniques: defining methodology and experimental protocols. – BBA-Bioenergetics **1367**: 88-106, 1998.

Koroidov S., Shevela D., Shutova T. *et al.*: Mobile hydrogen carbonate acts as proton acceptor in photosynthetic water oxidation. – P. Natl. Acad. Sci. USA **111**: 6299-6304, 2014.

Kuriata A.M., Chakraborty M., Henderson J.N. *et al.*: ATP and magnesium promote cotton short-form ribulose-1, 5-bisphosphate carboxylase/oxygenase (Rubisco) activase hexamer formation at low micromolar concentrations. – Biochemistry **53**: 7232-7246, 2014.

Lubitz W., Cox N., Rapatskiy L. *et al.*: Light-induced water oxidation in photosynthesis. – J. Biol. Inorg. Chem. **19**: S350-S350, 2014.

Roach T., Sedoud A., Krieger-Liszkay A.: Acetate in mixotrophic growth medium affects photosystem II in *Chlamydomonas reinhardtii* and protects against photoinhibition. – BBA-Bioenergetics **1827**: 1183-1190, 2013.

Rutherford A.W., Govindjee, Inoue Y.: Charge accumulation and photochemistry in leaves studied by thermo-luminescence and delayed light-emission. – P. Natl. Acad. Sci. USA **81**: 1107-1111, 1984.

Shen J.-R.: The structure of photosystem II and the mechanism of water oxidation in photosynthesis. – Annu. Rev. Plant Biol. **66**: 23-48, 2015.

Shevela D., Eaton-Rye J.J., Shen J.-R., Govindjee: Photosystem II and the unique role of bicarbonate: A historical perspective. – BBA-Bioenergetics **1817**: 1134-1151, 2012.

Shevela D., Su J.-H., Klimov V., Messinger J.: Hydrogencarbonate is not a tightly bound constituent of the water-oxidizing complex in photosystem II. – BBA-Bioenergetics **1777**: 532-539, 2008.

Snel J.F.H., van Rensen J.J.S.: Reevaluation of the role of electron flow in broken chloroplasts. – Plant Physiol. **75**: 146-150, 1984.

Stemler A.: Inhibition of photosystem II by formate. Possible evidence for a direct bicarbonate and formate in the regulation of photosynthetic role of bicarbonate in photosynthetic oxygen evolution. – BBA-Bioenergetics **593**: 103-112, 1980.

Stirbet A., Govindjee: On the relation between the Kautsky effect (chlorophyll *a* fluorescence induction) and photosystem II: basics and applications of the OJIP fluorescence transient. – J. Photoch. Photobio. B **104**: 236-257, 2011.

van Rensen J.J.S., Tonk W.J.M., de Bruijn S.M.: Involvement of bicarbonate in the protonation of the secondary quinone electron acceptor of photosystem II *via* the non-haem iron of the quinone-iron acceptor complex. – FEBS Lett. **226**: 347-351, 1988.

van Rensen J.J.S., Xu C., Govindjee: Role of bicarbonate in photosystem II, the water-plastoquinone oxido-reductase of plant photosynthesis. – Physiol. Plantarum **105**: 585-592, 1999.

Vermaas W.F., Rutherford A.W.: EPR measurements on the effects of bicarbonate and triazine resistance on the acceptor side of photosystem II. – FEBS Lett. **175**: 243-248, 1984.

Vinyard D.J., Zachary C.E., Ananyev G., Dismukes G.C.: Thermodynamically accurate modeling of the catalytic cycle of photosynthetic oxygen evolution: A mathematical solution to asymmetric Markov chains. – BBA-Bioenergetics **1827**: 861-868, 2013.

Vogt L., Ertem M.Z., Pal R. *et al.*: Computational insights on crystal structures of the oxygen-evolving complex of photosystem II with either Ca^{2+} or Ca^{2+} substituted by Sr^{2+}. – Biochemistry **54**: 820-825, 2015.

Vonshak A., Tomaselli L.: *Arthrospira* (*Spirulina*): systematics and ecophysiology. – In: Whitton B.A. (ed.): The Ecology of Cyanobacteria. Pp. 505-522. Springer, Dordrecht 2000

Wincencjusz H., van Gorkom H.J., Yocum C.F.: The photosynthetic oxygen evolving complex requires chloride for its redox state S2→ S3 and S3→ S0 transitions but not for S0→ S1 or S1→ S2 transitions. – Biochemistry **36**: 3663-3670, 1997.

Wydrzynski T., Govindjee: A new site of bicarbonate effect in photosystem II of photosynthesis: Evidence from chlorophyll fluorescence transients in spinach chloroplasts. – BBA-Bioenergetics **387**: 403-408, 1975.

Zarrouk C.: [Contribution to the study of Cyanophyceae, influence of various physical and chemical factors on growth and photosynthesis of *Spirulina maxima* (Setch and Gardner) Geitler.] – J. Univ de Paris, 1966. [In French]

Zhang H., Joseph J., Gurney M., *et al.*: Bicarbonate enhances peroxidase activity of Cu, Zn-superoxide dismutase role of carbonate anion radical and scavenging of carbonate anion radical by metalloporphyrin antioxidant enzyme mimetics. – J. Biol. Chem. **277**: 1013-1020, 2002.